A Theoretical Investigation of Substituent Effects on the Absorption and Emission Properties of a Series of Terpyridylplatinum(II) Acetylide Complexes

Xiao-Juan Liu,[a] Ji-Kang Feng,*[a,c] Jian Meng,[b] Qing-Jiang Pan,[a] Ai-Min Ren,[a] Xin Zhou,[a] and Hong-Xing Zhang[a]

Keywords: Density functional calculations / Electronic structure / N ligands / Platinum

A comprehensive calculational investigation has been carried out on a series of complexes of the type [(terpyridyl-R^1)-Pt(C≡C-R^2)], where terpyridyl-R^1 is a series of substituted 2,2′:6′,2′′-terpyridyl ligands and C≡C-R^2 is a series of substituted acetylide ligands. In one series of complexes (**I**), the energy of the electronic excited state is varied by changing the substituents on the terpyridyl ligand (R^1). In a second series of complexes (**II**), this electronic structure variation is obtained by changing the *para* substituents (R^2) of the acetylide ligand. The effect of varying the substituents on the lowest-energy excited states of the complexes has been assessed by calculating their electronic structures and excitation energies. We anticipated that introduction of electron-withdrawing substituents on the terpyridyl ligand will benefit the LLCT (or MLCT) and prohibit the nonradiative pathways via d-d transitions in these complexes; introduction of electron-donating substituents on the acetylide ligand can also prohibit the nonradiative pathways by increasing the energy gaps between the HOMO–LUMO and d-d transitions. The results also reveal that the lowest-energy excitations of all complexes of series **I** and **IIa–b** complexes are dominated by a π(C≡C)→π*(terp) (LLCT) transition mixed with some energetically dπ(Pt)→terpyridyl (MLCT) transition. However, for the complexes **IIc–IId**, in which phenyl rings are introduced on the acetylide ligand, the lowest-lying absorptions of **IIc** and **IId** are predominately LLCT in character, with less MLCT mixture, due to a lower contribution of the Pt(d) orbital to the HOMO, while for **IIe**, with a stronger donor on the acetylide, the lowest-lying absorption is completely LLCT in character. The absorption and emission calculations using the TDDFT method are based on the optimized geometries obtained at the B3LYP/LanL2DZ and CIS/LanL2DZ levels, respectively.

Introduction

Transition metal complexes that feature metal-to-ligand charge transfer (MLCT) excited states have fascinated photochemists for four decades.[1–12] This fascination derives from a combination of features exhibited by MLCT excited states, which include visible light absorption, photoluminescence, long lifetimes, and relative inertness toward unimolecular photochemistry.[9] By far the majority of the work that has been carried out on MLCT states has focused on d^6 metal–polypyridine complexes of Ru^{II}, Os^{II}, and Re^{I}.[8,9,13,14] However, recently there has been increasing interest in the properties of d^8 platinum(II) complexes such as [PtL_2(diimine)], where L = halide, nitrile, thiolate, isocyanide, and acetylide.[15–27] These Pt^{II}–diimine complexes feature long-lived excited states that are believed to be based on dπPt→π* diimine MLCT. Terpyridylplatinum(II) complexes have also attracted considerable attention in recent years, mainly because of their interesting spectroscopic behavior[28–33] and useful physical and biological properties.[34,35] Indeed, these complexes have been established as important DNA intercalators[34,36] and protein probes.[37] Their spectroscopic properties and low-energy absorptions generally arise from metal-to-ligand charge transfer (MLCT) transitions. However, the development of the photochemistry of these complexes is limited by their nonemissive or short-lived MLCT excited states in solution at room temperature.[28] This lack of emission originates from low-lying d-d excited states, which provide facile nonradiative deactivation pathways by molecular distortion. For these complexes, the d-d and MLCT excited sates are very close in energy, resulting in fast internal conversion from MLCT to d-d excited states. Many efforts have been performed to obtain emissive terpyridylplatinum(II) complexes with long-lived excited states and high emission quantum yields.[28–33] The main strategy to construct long-lived and emissive terpyridylplatinum(II) complexes involves utilizing substituted terpyridyl ligands with low-lying LUMOs and/or ancillary ligands on acetylide with a large electron-donating ability to raise the HOMO of the metal center, hence resulting in

[a] State Key Laboratory of Theoretical and Computational Chemistry, Institute of Theoretical Chemistry, Jilin University, Changchun 130023, P. R. China
[b] The Key Laboratory of Rare Earth Chemistry and Physics, ChangChun Institute of Applied Chemistry, Chinese Academy of Science, Changchun 130023, P. R. China
[c] The College of Chemistry, Jilin University, Changchun 130023, P. R. China

the reduction of the MLCT excited state energy. As a result, the energy difference between the MLCT and d-d state increases. Yam et al.[33] have synthesized a series of terpyridylplatinum(II) acetylide complexes and studied the absorption and emission properties of these complexes. They found that the emission energies depend on the nature of the acetylide ligands with different substituents on the phenyl ring, i.e., the more electron-withdrawing the group on the phenyl acetylide ligand, the higher the emission energy. This trend is consistent with an assignment of a triplet metal-to-ligand charge transfer (^{3}MLCT) state, probably mixed with some acetylide-to-terpyridine ligand-to-ligand charge transfer (^{3}LLCT) character. Tung et al.[38] have synthesized and investigated a series of 4-tolylterpyridylplatinum(II) acetylide complexes, which show high quantum yield and long lifetime photoluminescence from a triplet metal-to-ligand charge transfer (^{3}MLCT) excited state in fluid solution at room temperature. In their UV/Vis spectra, all the complexes exhibit intense vibronic-structure absorption bands at $\lambda < 350$ nm which come from the ligand-to-ligand (LLCT) transition of terpyridyl and acetylide ligands as well as the charge transfer transition involved in the Pt–C≡CR moieties, while the low-energy absorption bands at 400–500 nm are tentatively assigned to the $d\pi(Pt) \rightarrow \pi^*$(trpy) MLCT transition.

Our aim is to determine to what extent the substituents affect the low-lying electronic transitions of these complexes and thus assess the validity of the generally accepted MLCT assignments of the lowest-energy absorption bands. We hope that our theoretical investigation can provide an important guidance for the design of these metal coordination complexes. Two series of terpyridylplatinum(II) acetylide complexes have been studied. In one series, **Ia**–**Ic**, the substituents (R^1) on the tepyridyl ligand are varied (H, CH_3, and CN) while the structure of the acetylide ligands is held constant as -CH_2OH to investigate the effect of different terpyridyl substituents on the spectra; in the second series, **IIa**–**IIe**, the terpyridyl ligand is held constant (4-tolylterpyridyl) while the *para* substituents (R^2) on the acetylide ligands are varied (CH_2OH, *n*-propyl, C_6H_4Cl-4, C_6H_5, and -$C_6H_5NH_2$) to study the influence of different acetylide substituents. The electronic structures of the complexes were calculated by density functional theory, which was also used to determine the nature of the electronic transitions. The solvent effect was simulated by the polarizable continuum model (PCM).[39]

Results and Discussion

Ground-State Geometry Optimization

The complexes investigated are shown in Scheme 1. To provide the structures to be used for the calculation of the electronic spectra, ground-state geometry optimizations were first performed on the studied complexes. Because of the different substituents R^1 and R^2, the C_{2v} symmetry is broken and the entire molecular point group is reduced to C_1. Taking complex **IId** as an example, the perspective drawing is shown in Figure 1. Selected bond lengths and angles are tabulated in Table 1, along with the available experimental values of the X-ray crystal structure of complex **IId** for comparison.

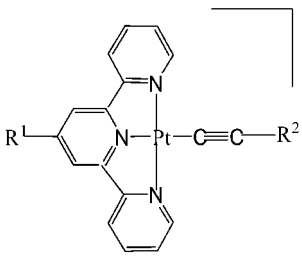

Ia: R^1 = H, R^2 = CH_2OH
Ib: R^1 = CH_3, R^2 = CH_2OH
Ic: R^1 = CN, R^2 = CH_2OH
IIa: R^1 = *p*-tolyl, R^2 = CH_2OH
IIb: R^1 = *p*-tolyl, R^2 = *n*-propyl
IIc: R^1 = *p*-tolyl, R^2 = C_6H_4Cl-4
IId: R^1 = *p*-tolyl, R^2 = C_6H_5
IIe: R^1 = *p*-tolyl, R^2 = $C_6H_4NH_2$-4

Scheme 1. Illustration of the investigated complexes.

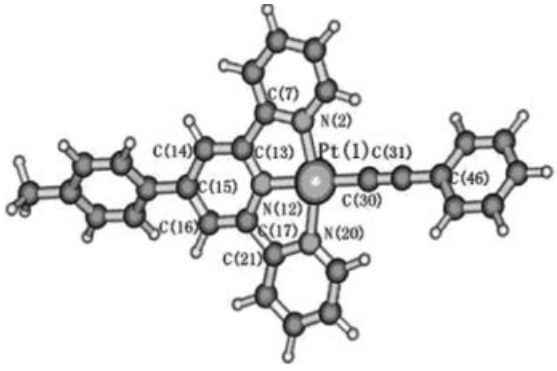

Figure 1. Complex structure and atom-numbering scheme taking complex **IId** as an example.

There is an overall satisfactory agreement between the theoretical and the available experimental data:[33] all the computed distances are within the experimental error (±0.04 Å). Table 1 shows that the variation of the substituents has more influence on the bond angles than on the bond lengths, as the bond lengths are almost unchanged while the bond angles undergo a comparatively large change. In particular, we should note the N(20)–Pt(1)–C(30) and Pt(1)–C(30)–C (31) angles, which show that when CH_2OH is connected to the acetylide ligand the Pt(1)–C(30)–C(31) angle deviates more from 180° (Table 1). This phenomenon is attributed to the weak interaction of CH_2OH with the Pt center. The coordination geometry about platinum is essentially square planar, with the bond length of the platinum to the central nitrogen atom [Pt(1)–N(12) = 1.99 Å] of the terpyridine ligand slightly shorter than to the other two outer nitrogen atoms [Pt(1)–N(2) and Pt(1)–N(20) are 2.05 Å and 2.04 Å, respectively], as required by the steric demands of the terpyridine ligand. These bond lengths are similar to the experimental[33] values of 1.97 Å, 2.01 Å, and 2.03 Å, respectively. Not surprisingly, the N–Pt–N angles [N(2)–Pt(1)–N(12) = 80.3°; N(12)–Pt(1)–N(20) = 80.3°; N(2)–Pt(1)–N(20) = 160.5°] deviate from the idealized values of 90° and 180° as a consequence of the geometric constraints imposed by the terpyridine ligand and the different substituents. The Pt–C bond length is 1.97 Å, which compares well with experimental

Table 1. Selected calculated bond lengths [Å] and bond angles [°] for all the complexes. The numbers in parentheses are from the X-ray crystal structure of complex **IId**.

Parameter	**Ia**	**Ib**	**Ic**	**IIa**	**IIb**	**IIc**	**IId**	**IIe**
Pt(1)–N(2)	2.05	2.05	2.05	2.05	2.05	2.05	2.05 (2.01)[a]	2.05
Pt(1)–N(12)	1.99	1.99	1.99	1.99	1.99	1.99	1.99 (1.97)	1.98
Pt(1)–N(20)	2.04	2.04	2.04	2.04	2.04	2.04	2.05 (2.03)	2.04
Pt(1)–C(30)	1.96	1.96	1.96	1.96	1.97	1.97	1.97 (1.98)	1.96
C(30)–C(31)	1.23	1.23	1.23	1.23	1.23	1.23	1.24 (1.19)	1.24
C(7)–C(13)	1.48	1.48	1.48	1.48	1.48	1.48	1.48	1.48
C(17)–C(21)	1.48	1.48	1.48	1.48	1.48	1.48	1.48	1.48
N(2)–Pt(1)–N(12)	80.6	80.7	80.7	80.4	80.4	80.2	80.3 (80.6)	80.4
N(12)–Pt(1)–N(20)	80.4	80.3	80.3	80.3	80.4	80.4	80.3 (81.0)	80.3
N(2)–Pt(1)–N(20)	161.2	161.0	161.0	160.8	160.6	160.6	160.5 (161.6)	160.7
N(12)–Pt(1)–C(30)	176.8	177.1	177.2	176.9	179.9	179.9	179.98 (178.8) 179.95	
N(2)–Pt(1)–C(30)	96.2	96.4	96.6	96.5	99.7	99.7	99.7 (99.5)	99.7
N(20)–Pt(1)–C(30)	102.7	102.6	102.5	102.8	99.6	99.7	99.7 (98.9)	99.7
Pt(1)–C(30)–C(31)	168.7	169.2	169.7	169.2	179.6	179.98	179.97 (179.10) 179.98	

[a] From ref.[33]

value of 1.98 Å.[33] The C≡C bond length of 1.22 Å is comparable to the experimental value of 1.19 Å.

Molecular Orbital Analysis

Since the observed differences in the chemical and physical properties of the complexes rely primarily on the changes in the ground-state electronic structure, before dealing with the excited states we will discuss in detail the ground-state electronic structure of these complexes with a special emphasis on the frontier orbital components, HOMO–LUMO energy gaps, and metal–metal transition energies. The calculated frontier orbital energies are tabulated in Table 2 and plotted according to their energy levels in Figure 2. The assignment of the nature of each MO was made on the basis of its components, as shown in Figure 3 and 4, taking complexes **Ib** and **IId** as examples, respectively. Through the contour plots of Figures 3 and 4, we can see that there is a degree of interaction between the π-orbitals of the terpyridyl and acetylide moieties via the Pt dπ-orbitals, and so the substituent effect on both ligands can extend across the Pt center and influence the excitation

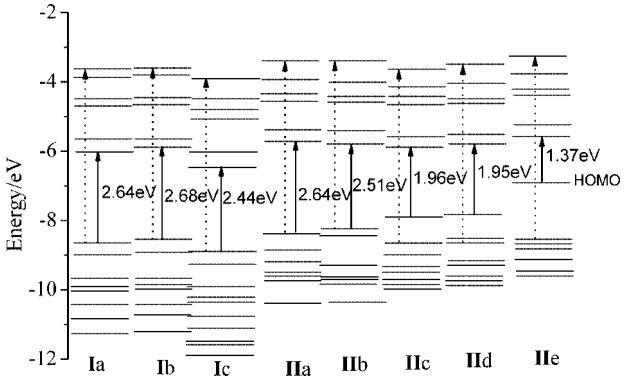

Figure 2. Molecular orbital energy level diagrams summarizing the B3LYP/LanL2DZ results. Solid and dotted arrows represent the energy gaps of HOMO and LUMO orbitals and that of d→d excitations.

nature of the complexes. A complete analysis of the highest occupied and lowest unoccupied molecular orbitals of all the complexes is presented in Table 3, where the orbital character and composition in terms of atomic contributions is presented. Percent contributions were calculated using

Table 2. Energies of the frontier molecular orbitals obtained from the B3LYP/LanL2DZ calculation.

Orbitals	**Ia**	**Ib**	**Ic**	**IIa**	**IIb**	**IIc**	**IId**	**IIe**
LUMO+5	–3.68	–3.58	–3.98	–3.45	–3.41	–3.60	–3.49	–3.27
LUMO+4	–3.94	–3.76	–4.59	–4.00	–4.02	–4.15	–4.06	–3.84
LUMO+3	–4.55	–4.47	–4.84	–4.38	–4.46	–4.58	–4.49	–4.28
LUMO+2	–4.72	–4.64	–5.12	–4.54	–4.53	–4.66	–4.57	–4.35
LUMO+1	–5.70	–5.61	–6.05	–5.42	–5.44	–5.57	–5.48	–5.26
LUMO	–6.03	–5.89	–6.50	–5.77	–5.78	–5.92	–5.83	–5.60
HOMO	–8.67	–8.57	–8.94	–8.41	–8.29	–7.88	–7.78	–6.97
HOMO–1	–9.07	–8.98	–9.34	–8.85	–8.48	–8.69	–8.63	–8.61
HOMO–2	–9.75	–9.68	–9.96	–9.24	–9.24	–8.99	–8.64	–8.68
HOMO–3	–9.93	–9.82	–10.25	–9.58	–9.65	–9.37	–9.26	–8.78
HOMO–4	–10.05	–9.94	–10.36	–9.65	–9.66	–9.49	–9.68	–9.11
HOMO–5	–10.50	–10.41	–10.81	–9.68	–9.79	–9.75	–9.73	–9.49
HOMO–6	–10.88	–10.72	–11.13	–9.81	–10.30	–9.83	–9.74	–9.55
HOMO–7	–11.31	–11.19	–11.52	–10.41	–11.01	–9.93	–9.86	–9.81
Energy gap	2.64	2.68	2.44	2.64	2.51	1.96	1.95	1.37

Equation (1), where n is the atomic orbital coefficient and $\sum n^2$ is the sum of the squares of all atomic orbital coefficients in a specific molecular orbital.

$$[n^2/\sum n^2] \times 100 = \%\ \text{contribution} \quad (1)$$

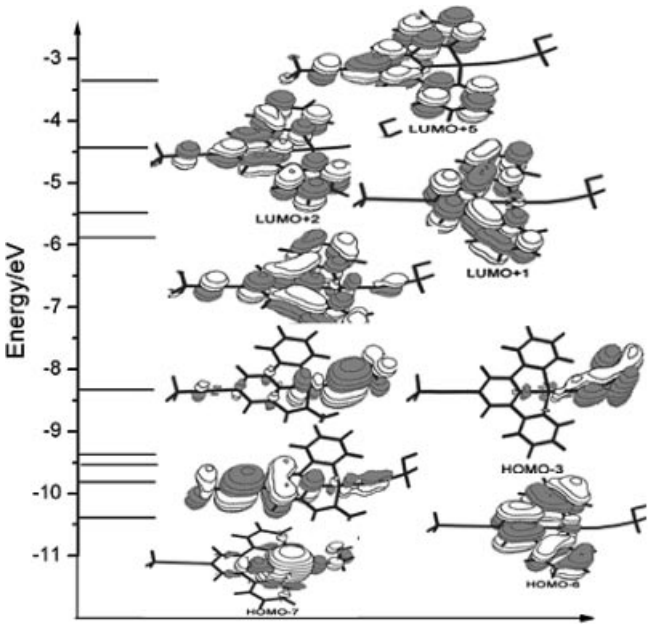

Figure 3. Frontier orbital diagram of complex **Ib** calculated at the B3LYP/LanL2DZ level. The plot on the right is the contour plot for each molecular orbital.

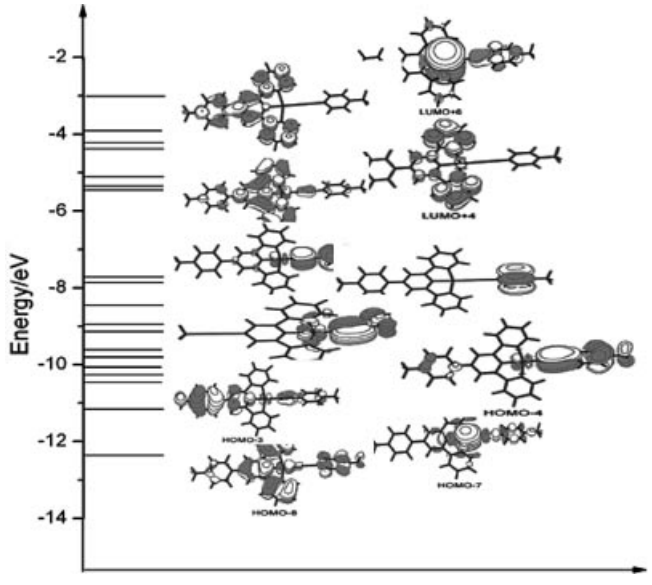

Figure 4. Frontier orbital diagram of complex **IId** calculated at the B3LYP/LanL2DZ level. The plot on the right is the contour plot for each molecular orbital.

Every complex is divided into three parts: the metal, the terpyridyl ligand with the substituent R^1, and the acetylide ligand with R^2. Each part of the percent contributions are the sum of the atomic coefficient squares.

In general, for all the investigated complexes, the first five unoccupied orbitals have the same character as the π*-orbital of the free terpyridyl ligand, although slightly perturbed by a small contribution from the d-orbital of Pt (about 6% for all the investigated complexes), and the LUMO+6 unoccupied orbitals are all composed of both Pt 3s and d_{z^2}orbitals and terpyridyl $2p_z$ orbitals. The low-energy transition character is therefore distinguished by the occupied orbital compositions. For series **I**, the occupied orbital compositions are perturbed by different substituted groups, but the relative ordering and characters are not changed: the HOMO orbitals have predominant -C≡C-R^2 character, mixed with Pt d-orbitals (24%, 37%, and 25% for **Ia**, **Ib** and **Ic**, respectively); the HOMO–3 and HOMO–7 orbitals are Pt- and terpyridyl-localized, respectively, and the HOMO–4 and HOMO–6 orbitals are a combination of Pt d-orbitals and terpyridyl π-orbitals (Table 3). Series **II** complexes can be separated into two groups: **IIa**,**b** (with -CH_2OH and -C_3H_7) in which the alkyl substituents are introduced on the acetylide and **IIc**–**e** in which phenyl rings are introduced on the acetylide. The HOMO orbitals for **IIa** and **IIb** have the same character as series **I** complexes, with predominant contributions from -C≡C-R^2 and some contributions from the Pt d-orbital (27% and 26%, respectively), while for **IIc**–**e** the HOMO orbitals are more –C≡C–R^2 in character due to the lower contributions from the Pt d-orbitals (8%, 10%, and 4% for **IIc**, **IId**, and **IIe**, respectively). In particular, the contribution of the Pt d-orbital to the HOMO (4%) in **IIe** is less than that to the LUMO (6%), so we characterized the HOMO in **IIe** as π(C≡C-R^2). It should be noted that introduction of a phenyl ring with a strong donor will lower the Pt d contribution to the HOMO (such as **IIc** and **IId**) or even change its character (such as **IIe**). According to the analysis of the frontier orbital compositions above, it can be found that the d-d excitations in complexes **Ia**–**c** and **IIa**,**b** occur between the HOMO to LUMO+6 transitions; while in complexes **IIc**–**e** the d-d excitations occur between the HOMO–1 to LUMO+6 transitions (see the dotted arrows in Figure 2).

We also investigated the substituent effects on the electronic orbital energy. Compared with those of complex **Ia**, the HOMO and LUMO molecular orbitals of **Ib** are lifted and the energy gap between the HOMO and LUMO ($\Delta E_{\text{HOMO–LUMO}}$) is increased ($\Delta E_{\text{HOMO–LUMO}}$ is 2.64 eV for **Ia** and 2.68 eV for **Ib**), while the HOMO and LUMO orbitals (especially the LUMO) of complex **Ic** are lowered greatly; the energy gap ($\Delta E_{\text{HOMO–LUMO}}$) decreases to 2.44 eV. According to the analysis above, the introduction of electron-withdrawing substituents on the terpyridyl ligands makes the HOMO→LUMO transition easier by lowering the $\Delta E_{\text{HOMO–LUMO}}$ energy gap, in particular by lowering the LUMOs, which are π* terpyridyl orbitals in this case. For the second series (**IIa**–**IIe**), it can be seen from Table 2 and Figure 2 that, first, compared with those of complexes **I**, the frontier molecular orbitals, especially the HOMOs, are lifted for all the series **II** complexes, and the energy gaps ($\Delta E_{\text{HOMO–LUMO}}$) are decreased further with the increase of the electron-donating ability of the substituents, and second, comparing the frontier orbitals of **IIc**, **IId**, and **IIe**, in which phenyl rings are included in the substituents,

Table 3. Calculated percentage composition of selected frontier MOs of complexes **Ia**–**IIe**, expressed in terms of component fragments.[a]

MO	Character	Pt	Terpyridyl	Acetylide	MO	Character	Pt	Terpyridyl	Acetylide
	Ia					**IIb**			
90(V)	Pt + terp	36	53	11	118(V)	Pt + terp	40	50	10
89(V)	terp	1	99		117(V)	terp		100	
88(V)	terp	2	98		116(V)	terp	3	97	
87(V)	terp	1	99		115(V)	terp		95	5
86(V)	terp	2	98		114(V)	terp	2	97	1
85(V)	terp	6	92	3	**113(V)**	terp	6	88	6
84(O)	Pt + C≡C–R^2	24	9	67	**112(O)**	Pt + terp	26	13	62
81(O)	Pt	96	3	1	110(O)	terp + R^1		95	5
80(O)	Pt + terp	63	37		107(O)	Pt + terp	64	36	
78(O)	Pt + terp	42	44	14	106(O)	terp	14	86	
77(O)	Pt + terp	22	75	3	102(O)	terp	14	84	2
	Ib					**IIc**			
94(V)	Pt + terp	36	53	10	129(V)	Pt + terp	35	53	11
93(V)	terp	1	96	3	128(V)	terp		100	
92(V)	terp	2	98		127(V)	terp	3	97	
91(V)	terp	2	98		126(V)	terp		100	
90(V)	terp	2	97	1	125(V)	terp	2	98	
89(V)	terp	6	91	3	**124(V)**	terp	6	93	1
88(O)	Pt++C≡C–R^2	37	13	50	**123(O)**	Pt+ C≡C–R^2	8	6	86
85(O)	Pt	97	2	1	122(O)	Pt+ C≡C–R^2	28	9	56
84(O)	Pt + terp	63	37		120(O)	R^1	1	89	10
82(O)	Pt + terp	43	42	15	115(O)	Pt + terp	62	38	
81(O)	terp	11	88	1	114(O)	Pt + terp	19	83	
112(O)	Pt+ C≡C–R^2	24	17	59					
111(O)	Pt + terp	17	80	3					
	Ic					**IId**			
96(V)	Pt + terp	37	53	10	126(V)	Pt + terp	36	54	10
95(V)	terp		100		125(V)	terp		100	
94(V)	terp	2	98		124(V)	terp	3	97	
93(V)	terp	1	98		123(V)	terp		100	
92(V)	terp	2	98		122(V)	terp	2	98	
91(V)	terp	7	90	3	**121(V)**	terp	6	92	
90(O)	Pt + C≡C–R^2	25	10	64	**120(O)**	Pt + C≡C-R^2	10	7	83
88(O)	C≡C–R^2	4	1	95	119(O)	R^2			100
87(O)	Pt	97	2	1	118(O)	Pt + C≡C-R^2	30	10	60
86(O)	Pt + terp	65	35	5	116(O)	Pt + terp	62	38	
85(O)	terp	12	88		114(O)	Pt + C≡C-R^2	21	9	65
84(O)	Pt + terp	27	42	14	113(O)	Pt + terp	62	38	
83(O)	terp	10	80	2	111(O)	Pt + terp + C≡C-R^2	39	35	20
80(O)	terp	17	62	2	109(O)	Pt + terp + C≡C-R^2	14	19	54
	IIa					**IIe**			
114(V)	Pt + terp	35	55	10	130(V)	Pt + terp	36	55	9
113(V)	terp		100		129(V)	terp		100	
112(V)	terp	2	98		128(V)	terp	2	98	
111(V)	terp	1	99		127(V)	terp	100		
110(V)	terp	2	98		126(V)	terp	2	98	
109(V)	terp	6	92	2	**125(V)**	terp	6	87	6
108(O)	Pt + C≡C-R^2	27	12	61	**124(O)**	C≡C-R^2	4	10	86
105(O)	C≡C-R^2	3	4	92	123(O)	Pt + C≡C-R^2	19	14	66
104(O)	R^1	2	97		121(O)	C≡C-R^2			99
102(O)	Pt + terp	62	38		119(O)	R^1		98	
100(O)	Pt + terp	39	46	15	116(O)	Pt + terp	20	80	
					115(O)	Pt + terp + C≡C-R^2	43	32	26
					114(O)	Pt + C≡C-R^2	3	74	23

[a] HOMO and LUMO orbitals are shown in bold.

with those of **IIa** and **IIb**, in which the substituents are only CH_2OH or C_3H_7, the energy gaps ($\Delta E_{HOMO–LUMO}$) are lower for **IIc**, **IId**, and **IIe**, thus indicating that introduction of a phenyl ring will enhance the HOMO→LUMO transition by virtue of the decreasing energy gaps ($\Delta E_{HOMO–LUMO}$). Finally, a comparison of the HOMO levels (see Table 2) and $\Delta E_{HOMO–LUMO}$ (see Table 2 and Figure 2) of complexes **IIa** and **IIb** shows that the donating ability of *n*-propyl is stronger than that of CH_2OH. Furthermore, in complexes **IIc**, **IId**, and **IIe** it is obvious

that the stronger donor group (NH_2 > H > Cl) on the phenyl rings leads to a greater decrease of the energy gaps ($\Delta E_{HOMO–LUMO}$ is 1.96 eV, 1.95 eV, and 1.37 eV for **IIc**, **IId**, and **IIe**, respectively).

The effect of the substituents on the electronic structures is described more quantitatively in Table 4, which lists the energy gaps of $\Delta E_{HOMO–LUMO}$, the d-d transition ($\Delta E_{d–d}$), and the energy difference between the HOMO–LUMO and the d-d transitions. The values of $\Delta E = \Delta E_{d-d} - \Delta E_{HOMO–LUMO}$ show that introduction of electron-withdrawing (donating) groups on the terpyridyl ligand makes this value larger (smaller) (in the first series this value is 2.35, 2.31, and 2.52 eV for complexes **Ia**, **Ib**, and **Ic**, respectively), and the introduction of electron-donating groups on the acetylide causes this value to increase (in the second series this value is 2.32, 2.37, 3.14, 3.19, and 3.97 eV for complexes **IIa**–**e**, respectively). As a result, with the increase of the energy difference between the HOMO–LUMO and the d-d transitions, the probability of nonradiative deactivation via the d-d state decreases. According to the analysis above, we can anticipate that the introduction of electron-withdrawing substituents on the terpyridyl ligand will benefit the LLCT (or MLCT) and prohibit the nonradiative pathways via d-d transitions in these complexes; the introduction of an electron-donating substituent on the acetylide ligand can also prevent the nonradiative pathways by increasing the energy gap between the HOMO–LUMO and d-d transitions. On the other hand, according to the energy gap law, the lower the energy of the excited state, the shorter the lifetime, so when we try to find effective light-emitting materials, we should consider these competing factors.

Table 4. The energy gaps (eV) of the $d\pi Pt \rightarrow d\pi^*Pt$ transitions ($\Delta E_{d–d}$) and HOMO → LUMO transitions ($\Delta E_{HOMO–LUMO}$), and the energy difference, ΔE, between them.

Complex	$\Delta E_{d–d}$	$\Delta E_{HOMO–LUMO}$	ΔE
Ia	4.99	2.64	2.35
Ib	4.99	2.68	2.31
Ic	4.96	2.44	2.52
IIa	4.96	2.64	2.32
IIb	4.88	2.51	2.37
IIc	5.09	1.96	3.14
IId	5.14	1.95	3.19
IIe	5.34	1.37	3.97

Absorption Properties

The low-energy absorption bands are very solvatochromic. To decrease the difference between calculated and observed transition energies, the effect of the solvent was simulated by the polarizable continuum model included in the Gaussian 98 program. In general, all these complexes show a blue-shift in the polarized solution, and this is in agreement with the recently published experimental data by Che et al.,[40] who pointed out that when the polarity of the solvent increases from benzene to CH_2Cl_2, acetonitrile, and ethanol, the broad low-energy absorption band blue-shifts in energy (a further explanation for this blue-shift is presented later). Taking molecule **IIa** as an example, the calculated absorptions in the gas phase and in dichloromethane solution are comparatively listed in Table 5. It can be seen that the first two absorptions show a comparatively strong solvatochromic effect − the 545 nm and 394 nm absorptions in the gas phase correspond to the 460 nm and 361 nm absorptions in solution, respectively − while the other absorptions show little solvatochromic effect. This phenomenon is in accordance with the experimental results.[28–33,38] The complete absorption spectrum for complex **IIa** is plotted in Figure 5 (in the plot, every absorption with different oscillator strength is selected, *f* is the oscillator strength, and the horizontal axis is the absorption wavelength).

Table 5. Selected calculated TDDFT singlet excitation energies for complex **IIa** in the gas phase and in CH_2Cl_2 solution, together with experimentally observed values.

G98/B3LYP		G98/B3LYP (PCM)		Exp.[a]		Transition designation
λ [nm]	Osc.	λ [nm]	Osc.	λ [nm]	ε [$M^{-1}cm^{-1}$]	
545	0.14	460	0.19	430	7260	LLCT+MLCT
394	0.12	361	0.17	342	19300	LLCT+MLCT
314	0.14	316	0.17	328	18000	LLCT
310	0.15	314	0.25	315	18500	MLCT+IL
269	0.20	272	0.29	274	35900	LLCT
257	0.31	265	0.20			LLCT
254	0.41	247	0.37			LLCT

[a] Taken from ref.[38]

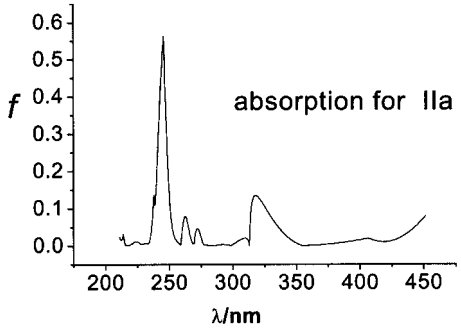

Figure 5. UV/Vis absorption spectrum of **IIa** in dichloromethane solution (*f* is the oscillator strength).

The calculated absorption results in dichloromethane solution from time-dependent DFT calculations (TDDFT) are listed in Table 6. In the first series, complexes **Ia**–**Ic**, introduction of a donor (CH_3 for **Ib**) on the terpyridyl ligands causes the absorptions to be blue-shifted (from 452 nm to 449 nm for the first absorption). This result is in accordance with the electronic-structure calculation results since introduction of an electron-donating group leads to the LUMO being lifted and the energy gap ($\Delta E_{HOMO–LUMO}$) being increased, which causes the absorption to be blue-shifted. This is consistent with the literature,[24] where the blue shift arising from methyl substitution of the bipyridyl ligand is attributable to destabilization of the π* level by electron-donating methyl substituents. The introduction of an electron-withdrawing group (CN) makes the absorption red-shift (from 452 nm to 487 nm for the first absorption). This result is also in accordance with

the electronic-structure calculations since introduction of electron-withdrawing groups on the terpyridyl ligands leads the LUMO to be lowered and the energy gap ($\Delta E_{HOMO-LUMO}$) to decrease, which results in the red-shift. In the second series of complexes, **IIa**–**IIe**, it can be seen that the stronger the electron-donating nature of the substituents on the acetylide, the more red-shifted the absorptions. This is because the stronger donating substituents on the acetylide raise the molecular HOMO (see Figure 2), and, as a result, the energy gap between the HOMO and LUMO decreases. The first absorption, which is mainly made up of the HOMO→LUMO transition, is red-shifted with an increase of the substituent group donating ability. Interestingly, all our calculated results and conclusions are in accordance with a recently published paper by Che et al.,[33,38] who ascribed the lower-energy band in the absorption spectra to an allowed MLCT transition. This assignment is consistent with the fact that the absorption band is red-shifted by electron-rich acetylide and electron-deficient moieties on diimine (C^N^N)-6-aryl-2,2′-bipyridine.

Table 6. Calculated absorptions (λ, nm) for the complexes in CH_2Cl_2 using the PCM model.

Ia	**Ib**	**Ic**	**IIa**
452 (0.08)	449 (0.09)	487 (0.12)	460 (0.19)/*430*[a]
407 (0.02)	409 (0.02)	426 (0.01)	414 (0.02)/*430*[a]
316 (0.29)	322 (0.03)	330 (0.14)	314 (0.17)/*342*[a]
246 (0.56)	313 (0.19)	253 (0.27)	314 (0.25)/*328*[a]
242 (0.41)	311 (0.12)	250 (0.26)	281 (0.15)/*289*[a]
263 (0.15)	230 (0.37)	247 (0.37)	
247 (0.44)			
241 (0.45)			
IIb	**IIc**	**IId**	**IIe**
480 (0.14)/*441*[a]	492 (0.20)	503 (0.11)/*482*[a]	742 (0.25)
395 (0.12)/*420*[a]	395 (0.12)	427 (0.14)/*433*[a]	399 (0.14)
324 (0.19)/*345*[a]	326 (0.10)	368 (0.12)/*342*[a]	359 (0.11)
309 (0.16)/*317*[a]	309 (0.17)	311 (0.18)/*317*[a]	311 (0.20)
260 (0.36)/*276*[a]	269 (0.31)	272 (0.25)/*289*[a]	286 (0.23)
255 (0.27)	256 (0.57)	260 (0.19)/*266*[a]	279 (0.41)
	252 (0.23)	252 (0.24)	
	245 (0.33)	245 (0.41)	

[a] Taken from ref.[38]

The excited states that arise from transitions between orbitals that are located on different moieties were classified as charge transfer (CT) excited states. Those from π-occupied to π-virtual orbitals located on the same ligand are described as π-π* states (IL), but those from orbitals on different ligands are described as ligand-to-ligand charge transfer (LLCT) states. Metal-to-ligand charge transfer (MLCT) states involve transitions from the metal atom to ligand-centered orbitals. The excited state is platinum centered (MC) if the orbitals involved in the transition are primarily located on the Pt atom.

In order to assign all absorption bands unambiguously, taking complexes **Ib** and **IId** as examples, TDDFT was used to calculate results for both singlet and triplet absorptions, as listed in Table 7. The contour plots for the related orbitals refer to Figure 3 and Figure 4. Commonly, an excited state corresponds to the excitation of an electron from an occupied to a virtual molecular orbital (MO). However, the excited states calculated herein demonstrate that excited-state electronic structures are described in terms of multi-electronic states, wherein a linear combination of several occupied-to-virtual molecular orbital excitations comprises a given optical transition. For simplicity, Table 7 lists only the most significant contributions to each excited state. Where multiple excitations are of comparable importance (i.e., several excitations with coefficients less 50%), each is listed. Assignment of the character of each excited state was based on the components of the occupied and virtual MOs of the dominant excitation(s) for that excited state. The absorptions **Ib** and **IId** are analyzed completely.

For complex **Ib**, it can be seen that the oscillator strengths of the two lowest-energy singlet electronic transitions are weak, which is consistent with the experimental results.[14] The lowest-energy absorption band is assigned to the spin-allowed HOMO→LUMO transition, which can be characterized as a π(C≡C)/d(Pt)→π*(terp) transition and thus as LLCT mixed with MLCT (LLCT/MLCT). The second absorption band (HOMO→LUMO+1) has the same character as the lowest-energy absorption. The third and sixth transitions, which mainly come from the transitions of HOMO–3→LUMO+1 and HOMO–3→LUMO+2, have complete MLCT character due to the predominant metal character of the HOMO–3 orbital. The other absorptions are all characterized as LLCT or IL. Within the calculated range no transitions between mainly platinum-centered orbitals (MC) are found. If they occur, they must therefore be higher in energy than 200 nm, according to our calculated results.

The first triplet excited state is positioned at 2.34 eV, and is therefore lower than the first singlet excited state (2.76 eV). It results from a HOMO to LUMO transition, thus it is featured as LLCT/MLCT. Similarly, the next two excited states are also characterized as LLCT/MLCT. The higher-energy transitions, such as those at 3.23 and 3.44 eV, arising from the transitions of HOMO–4 to the LUMO and HOMO–5 to LUMO, respectively, were assigned as intraligand excited states within the terpyridyl ligand (IL).

In complex **IId**, the first three calculated absorptions are much stronger than those of **Ib**; this is primarily due to the increased strong donating ability of the phenyl ring on the acetylide, which results in facile charge transfer during the excitation. The lowest-energy absorption (503 nm, with an oscillator strength of 0.1065), arising from the HOMO→LUMO transition, is assigned as LLCT/MLCT. Similarly, the 368 and 311 nm absorptions (with oscillator strengths 0.1243 and 0.1825, respectively) result from the HOMO–2→LUMO and HOMO–7→LUMO transitions, respectively, and they were characterized as mixed LLCT and MLCT due to the mixed compositions of HOMO–2 and HOMO–7 (HOMO–2 is made up of 30% Pt d, 10% terpyridyl p, and 60% acetylide p; HOMO–7 is 62% Pt d and s orbitals as well as 38% terpyridyl p orbitals). For the same reasons as for the 251 and 252 nm absorptions, they are also assigned as mixed LLCT and MLCT. The other absorptions (227, 260, and 245 nm) are all assigned as

Table 7. Selected TDDFT calculated excitation energies and compositions of the lowest-lying singlet and triplet excited states.

State	Composition		ΔE [eV]	λ [nm]	f	Character
Singlet (**Ib**)						
1	HOMO→LUMO	67%	2.76	450	0.0851	LLCT+MLCT
4	HOMO→LUMO+1	69%	3.03	409	0.0199	LLCT+MLCT
8	HOMO–3→LUMO+1	55%	3.85	322	0.0299	MLCT
10	HOMO–4→LUMO	52%	3.96	313	0.1912	ILCT
11	HOMO→LUMO+2	50%	3.98	318	0.1165	LLCT
24	HOMO–3→LUMO+2	51%	4.71	263	0.1524	MLCT
28	HOMO–6→LUMO+1	51%	5.01	247	0.4353	LLCT+ILCT
29	HOMO–7→LUMO	52%	5.14	241	0.4503	ILCT
Triplet (**Ib**)						
1	HOMO→LLUMO	71%	2.34	530		LLCT+MLCT
2	HOMO–2→LUMO	57%	2.90	428		LLCT+MLCT
4	HOMO→LUMO+1	58%	2.95	420		LLCT+MLCT
5	HOMO–2→LUMO+1	63%	3.02	409		LLCT+MLCT
6	HOMO–4→LUMO	71%	3.23	384		ILCT
7	HOMO–5→LUMO	70%	3.44	361		ILCT
Singlet (**IId**)						
1	HOMO→LUMO	68%	2.46	503	0.1065	LLCT+MLCT
2	HOMO–1→LUMO	63%	2.91	427	0.1438	LLCT
7	HOMO–2→LUMO	62%	3.37	368	0.1243	LLCT+MLCT
14	HOMO–7→LUMO	59%	3.98	311	0.1825	ILCT+MLCT
24	HOMO–1→LUMO+4	49%	4.56	272	0.2514	LLCT
	HOMO–6→LUMO+6	39%				
32	HOMO–6→LUMO+2	35%	4.77	260	0.1869	LLCT
	HOMO–4→LUMO+2	41%				
37	HOMO–9→LUMO+1	31%	4.92	252	0.1600	ILCT+MLCT
	HOMO–10→LUMO	28%				
38	HOMO→LUMO+5	29%	4.94	251	0.2257	LLCT+MLCT
	HOMO–2→LUMO+4	35%				
40	HOMO–11→LUMO	26%	5.07	245	0.3307	LLCT
	HOMO–3→LUMO+3	26%				
Triplet (**IId**)						
1	HOMO→LUMO	68%	2.23	555		LLCT+MLCT
2	HOMO–1→LUMO	66%	2.63	472		LLCT
3	HOMO→LUMO+1	65%	2.85	435		LLCT+MLCT
4	HOMO–4→LUMO	59%	2.90	427		ILCT
	HOMO–3→LUMO	34%				
5	HOMO–2→LUMO	67%	2.98	416		LLCT+MLCT
6	HOMO–4→LUMO+1	55%	3.08	403		ILCT
7	HOMO–6→LUMO	70%	3.19	389		LLCT+MLCT

LLCT between the $\pi(C{\equiv}C{-}R^2)$ and π^* (terp) orbitals. Again, within the calculated range no transitions between mainly platinum-centered orbitals (MC) were found. If they occur, they must be higher in energy than 200 nm.

The first triplet excited state is positioned at 2.23 eV, 0.23 eV lower than the first singlet excited state (2.46 eV). It results from a HOMO to LUMO transition, thus it is featured as LLCT/MLCT. Similarly, the third, fifth, and seventh excited states are also characterized as LLCT/MLCT. Other transitions, such as those at 2.63 and 3.08 eV, arise from the transitions of HOMO–1 to the LUMO and HOMO–4 to the LUMO+1, respectively, and were assigned as being due to ligand-to-ligand molecular charge transfer between the acetylide and terpyridyl ligand (LLCT). The 2.90 eV absorption, which comes from the HOMO–4 to LUMO transition, is characterized as IL.

According to the absorption character analysis of complexes **Ib** and **IId**, we can see that, although the transition character of HOMO to LUMO is the same for these two complexes (both are assigned as mixed LLCT/MLCT), the percentage of the MLCT is less in **IId** than that in **Ib**. However, his is not the case for the lowest-energy absorption of **IIe**. It should be noted that the Pt d orbital percentage in the HOMO (only 4%) is less than that of the LUMO (6%), so the lowest-energy transition, which comes from the HOMO to LUMO transition, should be assigned as LLCT.

Optimization of the Excited State

CIS (Configuration Interaction Singlets) has been extensively used to study the properties of excited states.[41–43] We

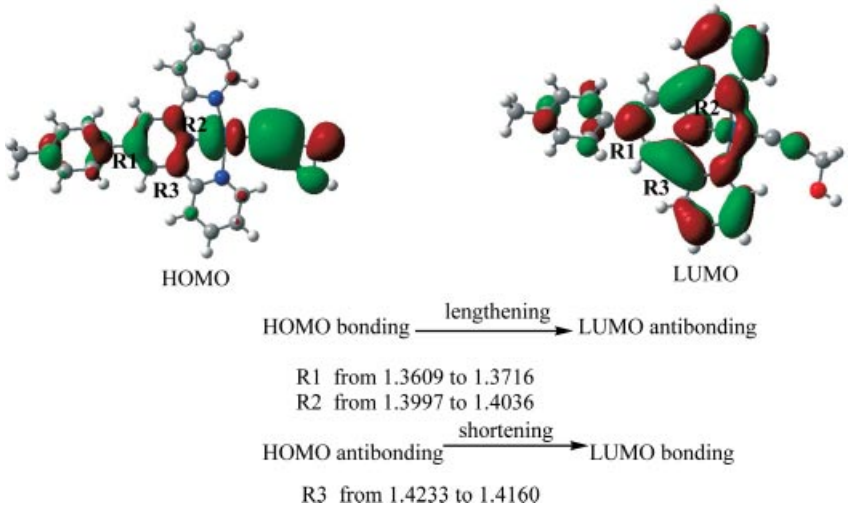

Figure 6. Prediction of the bond length changes between the ground and excited states according to the nodal of the frontier orbitals, taking complex **IIa** as an example (bond lengths in Å).

have examined the lowest triplet state of these complexes by carrying out CIS/LanL2DZ calculations. Comparing the optimized excited-state and ground-state geometries will provide an indication of overall geometry relaxations that occur in the excited state in possible emission processes. Taking complex **IIa** as an example, some of the geometrical parameters (bond lengths) for the optimized ground and excited states are shown in Figure 6. We investigated the geometry relaxations upon excitation by consideration of the nodal patterns of the HOMO and LUMO orbitals. It is considered that if there is no nodal across the bond in the HOMO, while there is a nodal across the same bond in the LUMO, then this bond will be elongated when the complex changes from the ground state to the excited state; in contrast, if there is no nodal across the bond in the LUMO, while there is a nodal across the same bond in the HOMO, then this bond will contract. According to this rule, we investigated the change in the bond lengths in complex **IIa**. The LUMO has nodes across R^1 and R^2, but there are no nodals across them in the HOMO. One would therefore expect elongation of these bonds, and Figure 6 shows that these bonds are in fact considerably longer in the excited state. The HOMO has a node across R^3, and it shows bonding in the LUMO; the data in Figure 6 confirm the anticipated contraction of this bond.

Solvatochromism is closely related to the ground- and excited-state dipole moment. Electronic excitations from HOMO to LUMO involve the displacement of electron charge from the Pt center and the C≡C-R^2 ligands towards the delocalized terpyridyl π*-orbitals. Thus, a reduction of the dipole moment in the excited state is expected, and, as a consequence, the excited state should be less stabilized by polar solvents than the ground state. To testify this assumption, we investigated the dipole moment of the ground and excited states. Taking complex **Ia** as an example, the ground-state dipole moment, μ_g, is –2.36 D and the first triplet excited-state dipole moment, μ_e, is 1.86 D, therefore $\Delta\mu$, the absolute difference between them, is 0.50 D. This dipole moment is in accordance with the assumptions above.

Emission Properties

Based on the optimized excited-state geometries of these complexes, the emission calculation was carried out using the TDDFT method at the B3LYP/LanL2DZ level. The emissions and the calculated Stokes shift are tabulated in Table 8, along with available experimental values for comparison. Obviously, the change tendency with the different substituents of emission is in parallel with those of absorption. The absolute emission value, taking **IId** as an example (693 nm), deviates from the experimental observation of 619 nm. We attribute this deviation to the following reasons: first, the excited-state geometries were obtained using CIS methods, and CIS represents excited states in a general zeroth-order method, just as Hartree–Fock for the ground state of molecular systems, and in CIS theory, the electron correlation effects and higher order excitations are neglected; in addition, the TDDFT approach neglects the spin–orbital coupling, which allows the triplet states to acquire intensity in both absorption and emission and to induce the triplet energies to be shifted. For third row transition metals one estimates the lowest triplet states to be low-

Table 8. Calculated emissions for all the investigated complexes in CH_2Cl_2 solvent, and their Stokes shifts.

Complex	Emission [λ, nm]	
	Calculated	Experiment
Ia	490	
Ib	471	
Ic	498	
IIa	489	552[a]
IIb	495	580[a]
IIc	589	619[a]
IId	693	

[a] Taken from ref.[38]

ered by 0.2–0.3 eV by interaction with higher states through spin–orbital coupling. However, the tendency of our calculated results changes parallel to the experimental ones, thus indicating that our method is reliable to gain reasonable results.

Conclusions

The ground-state geometries of several terpyridylplatinum(II) acetylide complexes have been calculated at the B3LYP/LanL2DZ level; the calculated geometrical parameters are in good agreement with the X-ray diffraction experiment results. The electronic structures are discussed completely. Introduction of electron-withdrawing groups on the terpyridyl ligand will lower the LUMO, and the introduction of electron-donating groups on the acetylide will raise the HOMO, thus decreasing the energy gap between the HOMO and the LUMO and, at the same time, increasing the energy gap between the lowest excited state and the d-d state, which prevents nonradiative deactivation through the pathways of d-d conversion. The absorptions and emissions for the investigated complexes were calculated at the B3LYP/LanL2DZ level at the optimized ground- and excited-state geometries, respectively. The calculated absorption results are in good agreement with the experimental values. For all the investigated complexes, excluding **IIe**, the lowest-energy absorption has been assigned as an admixture of metal-to-ligand transition to ligand-to-ligand transition (LLCT/MLCT-C≡C(π)/dπ(Pt)→trpy π*) (in **IIe** assigned as LLCT), while the absorptions at higher-energy levels are assigned as ligand-to-ligand charge transfer (LLCT) or IL. Furthermore, different substituents can modulate both the absorptions and emissions − the introduction of an acceptor on terpyridyl and a donor on acetylide induces the absorption and emission to be red-shifted. This result is in accordance with the calculated electronic structure.

The introduction of electron-withdrawing groups on the terpyridyl ligand and electron-donating groups on the acetylide ligand benefits the emission of this series of complex since it decreases the energy gap between the HOMO and the LUMO and increases the energy gap between the d-d transitions.

Computational Methods

Calculations on the electronic ground state of the investigated complexes were carried out using B3LYP density functional theory. B3LYP corresponds to the combination of Becke's three-parameter exchange functional (B3) with the Lee–Yang–Parr for the correlation functional (LYP). A LanL2DZ basis set was used for all the elements, including C, N, O, H, and Pt atoms. A relativistic effective core potential (ECP) on Pt replaced the inner-core electrons, leaving the outer-core [($5s^2$) ($5p^6$)] electrons and the ($5d^8$) valence electrons of Pt. For the C, N, and O atoms only the (1s) orbitals were replaced by effective core potentials; all the other orbital electrons were left as outer-core electrons or valence electrons. The basis sets were taken as Pt (8s6p3d/3s3p2d), C (10s5p/3s2p), N (10s5p/3s2p), O (10s2p/3s2p), and H (4s/2s). The equilibrium ground-state geometries were computed using the B3LYP functional with the LanL2DZ basis set and were fully optimized without symmetry constraints. At the correct ground-state geometry optimizations, time-dependent DFT (TDDFT) calculations using the B3LYP functional were performed to obtain both singlet and triplet absorption spectra. Then, the first triplet excited state (T_1) geometries for all the complexes (except for complex **IIe**) were optimized using an ab initio CIS method with the LanL2DZ basis set. Based on the CIS-optimized excited-state geometries, the luminescent spectra were calculated at the B3LYP/LanL2DZ level. The solvent effect was simulated using the polarizable continuum model (PCM), in which the solvent cavity is seen as a union of interlocking atomic spheres. All the calculations described here were carried out with the Gaussian 98 package.[44]

Acknowledgments

This work was supported by the Major State Basis Research Development Program (no. 2002CB 613406), the National Nature Science Foundation of China (no. 90101026 20173021), and the National Natural Science Foundation of China (no. 20271049 and 20331030).

[1] J. P. Paris, W. W. Brandt, *J. Am. Chem. Soc.* **1959**, *81*, 5001–5002.
[2] J. N. Demas, G. A. Crosby, *J. Mol. Spectrosc.* **1968**, *26*, 72–77.
[3] G. D. Hager, G. A. Crosby, *J. Am. Chem. Soc.* **1975**, *97*, 7031–7037.
[4] G. D. Hager, R. J. Watts, G. A. Crosby, *J. Am. Chem. Soc.* **1975**, *97*, 7037–7042.
[5] K. W. Hipps, G. A. Crosby, *J. Am. Chem. Soc.* **1975**, *97*, 7042–7048.
[6] J. Van Houten, R. J. Watts, *J. Am. Chem. Soc.* **1976**, *98*, 4853–4858.
[7] T. J. Meyer, *Prog. Inorg. Chem.* **1983**, *30*, 389–440.
[8] J. V. Caspar, T. J. Meyer, *J. Phys. Chem.* **1983**, *87*, 952–957.
[9] A. Juris, V. Balzani, F. Barigelletti, S. Campagna, P. Belser, A. von Zelewsky, *Coord, Chem. Rev.* **1988**, *84*, 85–277.
[10] A. T. Yeh, C. V. Shank, J. K. McCusker, *Science* **2000**, *289*, 935–938.
[11] M. Wrighton, D. L. Morse, *J. Am. Chem. Soc.* **1974**, *96*, 998–1003.
[12] A. J. Lees, *Chem. Rev.* **1987**, *87*, 711–743.
[13] J. V. Caspar, E. M. Kober, B. P. Sullivan, T. J. Meyer, *J. Am. Chem. Soc.* **1982**, *104*, 630–631.
[14] L. A. Worl, R. Duesing, P. Chen, L. D. Ciana, T. J. Meyer, *J. Chem. Soc., Dalton Trans.* **1991**, 849–858.
[15] V. M. Miskowski, V. H. Houlding, *Inorg. Chem.* **1989**, *28*, 1529–1533.
[16] H. Kunkely, A. Vogler, *J. Am. Chem. Soc.* **1990**, *112*, 5625–5627.
[17] V. M. Miskowski, V. H. Houlding, C. M. Che, Y. Wang, *Inorg. Chem.* **1993**, *32*, 2518–2524.
[18] C. W. Chan, L. K. Cheng, C. M. Che, *Coord. Chem. Rev.* **1994**, *132*, 87–97.
[19] S. D. Cummings, R. Eisenberg, *J. Am. Chem. Soc.* **1996**, *118*, 1949–1960.
[20] Y. Zhang, K. D. Ley, K. S. Schanze, *Inorg. Chem.* **1996**, *35*, 7102–7110.

[21] W. B. Connick, H. B. Gray, *J. Am. Chem. Soc.* **1997**, *119*, 11 620–11 627.
[22] W. Paw, S. D. Cummings, M. A. Mansour, W. B. Connick, D. K. Geiger, R. Eisenberg, *Coord. Chem. Rev.* **1998**, *171*, 125–150.
[23] W. B. Connick, D. Geiger, R. Eisenberg, *Inorg. Chem.* **1999**, *38*, 3264–3265.
[24] W. B. Connick, V. M. Miskowski, V. H. Houlding, H. B. Gray, *Inorg. Chem.* **2000**, *39*, 2585–2592.
[25] M. Hissler, W. B. Connick, D. K. Geiger, J. E. McGarrah, D. Lipa, R. J. Lachiocotte, R. Eisenberg, *Inorg. Chem.* **2000**, *39*, 447–457.
[26] M. Hisser, J. E. McGarrah, W. B. Connick, D. K. Geiger, S. D. Cummings, R. Eisenberg, *Coord. Chem. Rev.* **2000**, *208*, 115–137.
[27] C. J. Adams, S. L. James, X. M. Liu, P. R. Raithby, L. J. Yellowlees, *J. Chem. Soc., Dalton Trans.* **2000**, 63–67.
[28] J. F. Michalec, S. A. Bejune, D. G. Cuttell, G. C. Summerton, J. A. Gertenbach, J. S. Field, R. J. Haines, D. R. McMillin, *Inorg. Chem.* **2001**, *40*, 2193–2200.
[29] S. W. Lai, M. C. W. Chan, K. K. Cheung, C. M. Che, *Inorg. Chem.* **1999**, *38*, 4262–4267.
[30] R. Büchner, C. T. Cunningham, J. S. Field, R. J. Haines, D. R. McMillin, G. C. Summerton, *J. Chem. Soc., Dalton Trans.* **1999**, 711–717.
[31] R. Büchner, J. S. Field, R. J. Haines, C. T. Cunningham, D. R. McMillin, *Inorg. Chem.* **1997**, *36*, 3952–3956.
[32] J. F. Michalec, S. A. Bejune, D. R. McMillin, *Inorg. Chem.* **2000**, *39*, 2708–2709.
[33] V. W. W. Yam, R. P. L. Tang, K. M. C. Wong, K. K. Cheung, *Organometallics* **2001**, *20*, 4476–4482.
[34] S. Lippard, *Acc. Chem. Res.* **1978**, *11*, 211–217.
[35] C. S. Peyratout, T. K. Aldridge, D. K. Crites, D. R. McMillin, *Inorg. Chem.* **1995**, *34*, 4484–4489.
[36] G. Arena, L. Monsú Scolaro, R. F. Pasternack, R. Romeo, *Inorg. Chem.* **1995**, *34*, 2994–3002.
[37] E. M. A. Ratilla, H. M. Brothers, N. M. Kostić, *J. Am. Chem. Soc.* **1987**, *109*, 4592–4599.
[38] Q. Z. Yang, L. Z. Wu, L. P. Zhang, C. H. Tung, *Inorg. Chem.* **2002**, *41*, 5653–5655.
[39] C. Amovilli, V. Barone, R. Cammi, E. Cances, M. Cossi, B. Mennucci, C. S. Pomelli, J. Tomasi, *Adv. Quantum Chem.* **1999**, *32*, 227.
[40] W. Lu, B. X. Mi, C. W. Michael, Z. Hui, C. M. Che, N. Y. Zhu, S. T. Lee, *J. Am. Chem. Soc.* **2004**, *126*, 4958–4971.
[41] Q. J. Pan, H. X. Zhang, *J. Chem. Phys.* **2003**, *119*, 4346–4352.
[42] Q. J. Pan, H. X. Zhang, *Eur. J. Inorg. Chem.* **2003**, *23*, 4202–4210.
[43] Q. J. Pan, Zhang, H. X, *Inorg. Chem.* **2004**, *43*, 593–601.
[44] M. J. Frisch, G. W. Trucks, H. B. Schlegel, G. E. Scuseria, M. A. Robb, J. R. Cheeseman, V. G. Zakrzewski, J. A. Montgomery, R. E. Stratmann, J. C. Burant, S. Dapprich, J. M. Millam, A. D. Daniels, K. N. Kudin, M. C. Strain, O. Farkas, J. Tomasi, V. Barone, M. Cossi, R. Cammi, B. Mennucci, C. Pomelli, C. Adamo, S. Clifford, J. Ochterski, G. A. Petersson, P. Y. Ayala, Q. Cui, K. Morokuma, D. K. Malick, A. D. Rabuck, K. Raghavachari, J. B. Foresman, J. Cioslowski, J. V. Ortiz, B. B. Stefanov, G. Liu, A. Liashenko, P. Piskorz, I. Komaromi, R. Gomperts, R. L. Martin, D. J. Fox, T. Keith, M. A. AI-Laham, C. Y. Peng, A. Nanayakkara, C. Gonzalez, M. Challacombe, P. M. W. Gill, B. G. Johnson, W. Chen, M. W. Wong, J. L. Andres, M. Head-Gordon, E. S. Replogle, J. A. Pople, *Gaussian 98*, revision A.9; Gaussian, Inc.: Pittsburgh, PA, **1998**.

Received: June 18, 2004

